Annals of Biomedical Engineering, Vol. 29, pp. 121–127, 2001
Printed in the USA. All rights reserved.

0090-6964/2001/29(2)/121/7/$15.00

Mass Transport in an Anatomically Realistic Human Right Coronary Artery

M. R. KAAZEMPUR-MOFRAD and C. R. ETHIER

Department of Mechanical and Industrial Engineering, University of Toronto, Toronto, Ontario, Canada M5S 3G8

(Received 15 February 2000; accepted 19 December 2000)

Abstract—The coronary arteries are a common site of atherosclerotic plaque formation, which has been putatively linked to hemodynamic and mass transport patterns. The purpose of this paper was to study mass transport patterns in a human right coronary artery (RCA) model, focusing on the effects of local geometric features on mass transfer from blood to artery walls. Using a previously developed characteristic/finite element scheme for solving advection-dominated transport problems, mass transfer calculations were performed in a rigid, anatomically realistic model of a human RCA. A qualitative and quantitative examination of the RCA geometry was also carried out. The concentration field within the RCA was seen to closely follow primary and secondary flow features. Local variations in mass transfer patterns due to geometric features were significant and much larger in magnitude than local variations in wall shear stress. We conclude that the complex secondary flows in a realistic arterial model can produce very substantial local variations in blood-wall mass transfer rates, and may be important in atherogenesis. Further, RCA mass transfer patterns are more sensitive to local geometric features than are wall shear stress patterns. © *2001 Biomedical Engineering Society.*
[DOI: 10.1114/1.1349704]

Keywords—Mass transport, Right coronary artery, Atherosclerosis, Hemodynamics, Modeling

INTRODUCTION

Atherosclerosis is the leading cause of morbidity and mortality in Western societies. Fluid dynamic and mass transfer related phenomena have been hypothesized to contribute to the initiation and progression of atherosclerosis.[2,3,7,8,12,14,18] For example, mass transfer effects have been shown to influence endothelial function, specifically the response of vascular endothelium to circulating ATP.[4] Local variations in mass transfer efficacy, if translated into alterations in local endothelial behavior, could be an important factor in the localization of atherosclerotic lesion development. In order to assess possible links between atherogenesis and hemodynamic and mass transport patterns, accurate characterization of local flow and mass transport features is required.

When considering mass transfer between flowing blood and the artery wall, the species of interest have a range of sizes, from small (e.g., oxygen) to very large (e.g., lipoproteins, particularly LDLs). This is anatomically and biomechanically different from blood-to-tissue mass transfer at the capillary level, where the transported species are primarily low molecular weight substances such as oxygen, glucose, CO_2, etc. Tissue level mass transfer is clearly central to maintenance of normal myocardial metabolism, but is not the focus of this paper. Instead, we focus on transfer from the blood to the artery wall, and its implications for atherogenesis in the coronary arteries. More specifically, the focus of this paper is on the fluid-side mass transport, and to this end, we consider species that have a relatively large blood-side mass transfer resistance and hence their transport is not expected to be rate limited by wall-side processes.

Arterial geometry strongly influences coronary artery flow patterns.[6] In a companion article, Myers *et al.*[13] describe the flow in the present anatomically realistic right coronary artery (RCA) model and report a sensitive dependence of wall shear stress patterns on compound curvature. Mass transfer patterns in an idealized coronary artery modeled as a curved tube also show important geometric effects, including large differences in the value of Sherwood number between the inner and outer wall.[18]

The objective of this paper is to study mass transport patterns in a realistic RCA model, and to comment on factors affecting mass transport from blood to the artery wall. This paper is in some sense an extension of the earlier work of Qiu and Tarbell[18] that includes a more complex arterial geometry. We show that the inclusion of realistic geometric effects dramatically influences mass transport.

Address correspondence to Professor C. Ross Ethier, Department of Mechanical and Industrial Engineering, University of Toronto, 5 King's College Road, Toronto, Ontario, Canada M5S 3G8. Electronic mail: ethier@mie.utoronto.ca

METHODS

An anatomically faithful model of the right coronary artery of a 47 year old female who died from noncardiovascular related causes was constructed as described in the companion paper.[13]

Flow and Mass Transfer Solution

The RCA model was assumed to be stationary with rigid walls. Obviously, the coronary arteries (which lie on the surface of the heart) move as the heart beats, leading to a dynamically changing arterial curvature. Also, flow pulsation and pressure variations cause the distensible artery to dynamically change its cross-sectional area. Further studies must be carried out to investigate the effects of artery movement and distensibility.

Blood was assumed to have Newtonian rheology. The non-Newtonian viscosity of blood has been found to have little effect on the dynamics of blood flow in the large arteries of interest.[1]

Three-dimensional (3D), steady, incompressible flow at a Reynolds number of $\mathrm{Re}_D=500$ (based on the inlet diameter) was first simulated in the RCA model, the details of which are given in Ref. 13. The flow boundary conditions were as follows: a fully developed (Poiseuille) velocity profile was imposed at the inlet, the no-slip velocity boundary condition was set on the walls, and the traction-free boundary condition was applied at the outlet. The mesh used for flow simulation contained 108,036 nodes and 65,416 quadratic ten-noded Taylor–Hood tetrahedral finite elements.

The 3D steady advection-diffusion equation was then solved using a characteristic/finite element algorithm.[10,11] Simulations were carried out at Schmidt numbers ($\mathrm{Sc}=\nu/\mathscr{D}$) of 3000, which is representative of relatively small species such as ATP, or for free oxygen in blood. This corresponds to a Peclet number of $\mathrm{Pe}_D=1.5\times10^6$. The following mass transfer boundary conditions were imposed on the dimensionless concentration, c, defined as $c=(c^*-c_w^*)/(c_i^*-c_w^*)$ where c^* is the dimensional concentration, and subscripts $_w$ and $_i$ denote wall and inlet, respectively. A uniform dimensionless concentration of $c=1$ was imposed at the inlet, a Dirichlet boundary condition of $c=0$ was set on the walls, and a zero gradient in c was applied at the outlet.

In highly advection-dominated transport problems, the boundary layer is very thin throughout the whole domain, except in regions of flow separation. To resolve such thin boundary layers, while keeping the mesh size within practical limits, stretched (high aspect ratio) elements are needed. We previously developed a general strategy for generating stretched tetrahedral elements in the boundary (high gradient) regions of a domain. Details of this technique can be found in Ref. 9. Briefly, using the boundary (wall) mesh used in flow calculations, layer(s) of prismatic elements are first generated with triangular bases adjacent to the wall. Then, each prism is subdivided into either three or eight tetrahedra depending on the surrounding mesh topology. The remainder of the domain, i.e., that not immediately adjacent to the wall, was meshed directly with tetrahedra. In this study, we generated two meshes in order to check the mesh dependence of the solution. The coarser mesh contained 311,915 linear tetrahedral elements with 63,889 corner nodes. The off-wall spacing was approximately 1/400th of the inlet diameter. The finer mesh had 405,114 four-noded (linear) tetrahedral elements with 71,741 corner nodes. Figure 1 shows a slice through the finer mesh near the boundary wall. The off-wall spacing was about 1/500th of the inlet diameter.

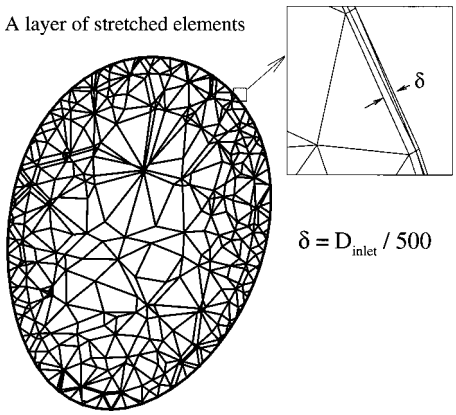

FIGURE 1. A slice through the mass transfer mesh.

The flow field solution was interpolated from the flow mesh onto the mass transfer mesh by using the finite element velocity basis functions. For wall nodes, and the nodes which were at the inlet, we directly assigned the appropriate velocity based on known boundary conditions.

RESULTS

Arterial Geometry Analysis

The complex geometry of the RCA model strongly affects hemodynamic and mass transport effects, and we therefore review it in detail here. A qualitative examination of the RCA (Fig. 1 of Ref. 13) shows that the RCA exhibits appreciable 3D variations in curvature and cross section. It is evident that the curvature seen in the medial plane is more pronounced than the curvatures in the ventral and frontal planes. The curvature within the medial plane will be therefore denoted as the ''primary curvature,'' while the out-of-plane curvatures will be denoted as ''secondary curvatures.''

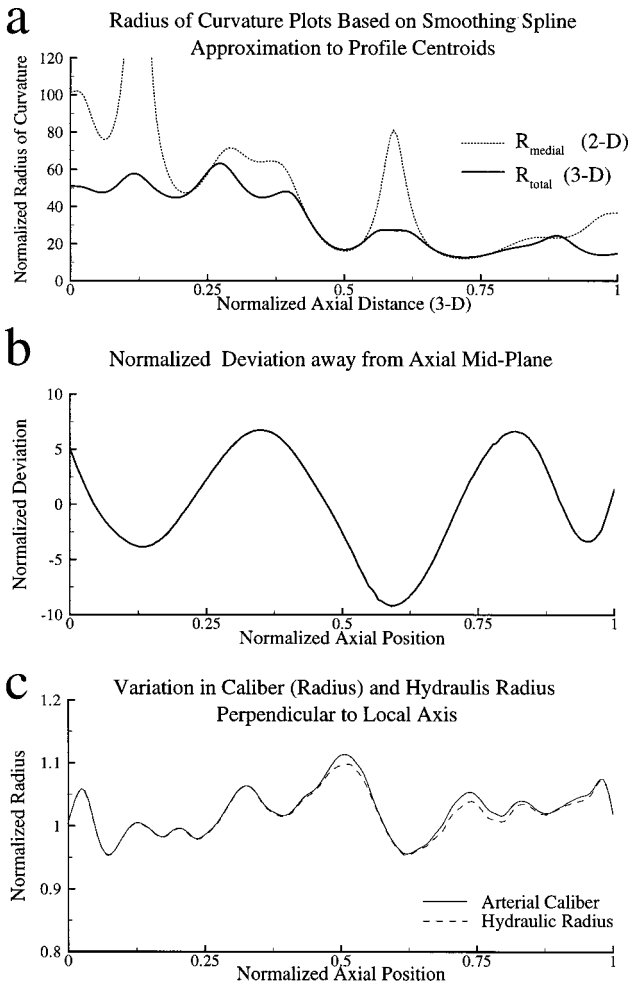

FIGURE 2. Geometry specifications of the RCA model. The radius of curvature, normalized deviation, the arterial caliber, and the hydraulic radius are all normalized by the RCA inlet radius a. The axial position is normalized by the total 3D length of the RCA. The radius of curvature, R_{medial}, was calculated using a spline approximation to the centroidal path. The arterial radius (caliber) is the the radius of an equivalent circular area.

A quantitative illustration of the RCA curvature along the artery is given in Fig. 2(a) where the total (i.e., 3D) radius of curvature along the RCA centroidal path is compared to the radius of the curvature in the medial plane. The centroidal path is the curve that passes through the centroids of consecutive cross-sectional profiles (see the Model Construction procedure in Ref. 13). The total (i.e., 3D) radius of curvature, R_{total}, was obtained from a spline approximation to this centroidal path. The medial (i.e., 2D) radius of curvature, R_{medial}, was calculated using the projection of the centroidal path on the medial plane. R_{total} and R_{medial} were both normalized by RCA inlet radius. As evident in Fig. 2(a), the curvature in the medial plane substantially contributes to the overall curvature of the artery [note the similar distribution and amplitude of R_{medial} (2D) and R_{total} (3D) over much of the artery length]. However, in several locations the total radius of curvature R_{total} is several times smaller than the medial radius of curvature. In these regions, the RCA path in the medial plane is nearly straight, and the secondary (out-of-plane) curvatures represent the principal curvature effects.

Other signs of complexity of the RCA geometry are the deviation of the RCA path relative to the medial plane and the local variations in cross-sectional area [Figs. 2(b) and 2(c)]. Using the axial midplane as a reference location, the RCA ''normalized deviation'' shows a relatively sinusoidal distribution with an amplitude of approximately $\pm 5a$, where a is the radius of the artery at the inlet. The arterial cross-section area also varies along the artery length. We characterized this variation by plotting normalized arterial caliber, defined as the radius of a circle with an area equivalent to that of the artery cross section normalized by the inlet radius [see Fig. 2(c)]. This normalized radius is seen to vary continuously throughout the arterial path, with a maximum increase and decrease of 11% and 3%, respectively.

In general, the shape of the cross section is neither circular nor consistent along the artery path, as characterized by the variation in the hydraulic radius [Fig. 2(c)]. The normalized hydraulic radius is nearly identical to the local arterial caliber (radius of an equivalent circular area) in the inlet regions of the RCA. However, further downstream the hydraulic radius drops below the arterial caliber, marking regions where the artery shape deviates from circular.

An important fluid mechanical factor is the Dean number, defined as $D_n=(a/R)^{1/2}\,\mathrm{Re}_D$, where a/R is the radius ratio, i.e., arterial caliber over 3D radius of curvature.[17] Using a Reynolds number of $\mathrm{Re}_D=500$, the local effective Dean number for this geometry ranged approximately between 60 and 145 (see Fig. 3). Fluid mechanically, this range of Dean numbers represents the intermediate regime in which the inertial, viscous, and centrifugal forces are all of similar importance.[16]

Flow Field

Velocity profiles in the RCA are strongly influenced by arterial curvature and are described in detail in the companion paper.[13]

Mass Transfer Patterns

Grid Sensitivity. Grid sensitivity was investigated by comparing the dimensionless concentration gradient (or Sherwood number) distribution on the inner and outer walls in the two meshes described in the Flow and Mass Transfer Solution section. The Sherwood number, Sh_D, is defined as $\mathrm{Sh}_D=[h_c(2a)/\mathscr{D}]$, where h_c is the local

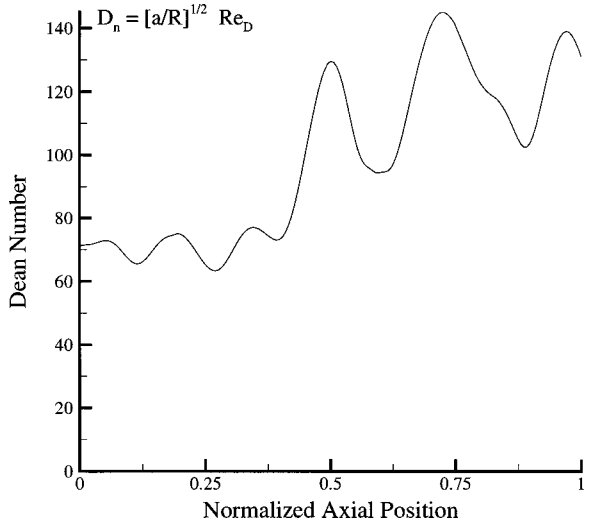

FIGURE 3. Dean number variations along the arterial length for an inlet Re_D=500.

mass transfer coefficient, a is the (dimensional) inlet radius, and $\mathscr{D}$ is the diffusion coefficient. This is equivalent to $Sh_D = 2\nabla c \cdot \mathbf{n}$, where c is the normalized concentration as previously defined, and $\mathbf{n}$ is the inward unit vector normal to the wall. The quantity ∇c is calculated at the wall by analytic differentiation of the finite element basis functions and substitution of nodal values of c from elements with faces on the wall.

The Sherwood number, Sh_D, distributions on the inner and outer walls of the RCA model are shown in Fig. 4. Along the RCA inner wall, the Sh_D distributions have very close qualitative and quantitative patterns in the two meshes. We conclude that our mesh is able to reasonably accurately capture the inner wall Sh_D distribution. The outer wall Sh_D distribution, however, showed some mesh dependence between the coarse and fine meshes. This indicates that the mesh is not fully resolving the outer wall concentration gradient. Nevertheless, the qualitative trend of the outer wall Sherwood number is captured. Considering that most of the disease formation occurs in the proximal region of the RCA inner wall,[5,15] as well as the computational cost required for further refining the mesh, the finer mesh can be considered sufficient for the purposes of this study. Work is currently underway to extend the present characteristic/finite element scheme for solving the advection-diffusion equation to higher order tetrahedral elements which provide a higher node to element ratio and, hence, can offer better boundary resolution with minimal extra computational cost.

Isoconcentration Contours. Fluid regions with high axial momentum were often associated with higher species concentration, while low concentration areas were formed in regions of low momentum fluid (Fig. 5). The ''horse shoe'' shape of the high concentration fluid, especially for axial distances between 0.4 and 0.7, showed

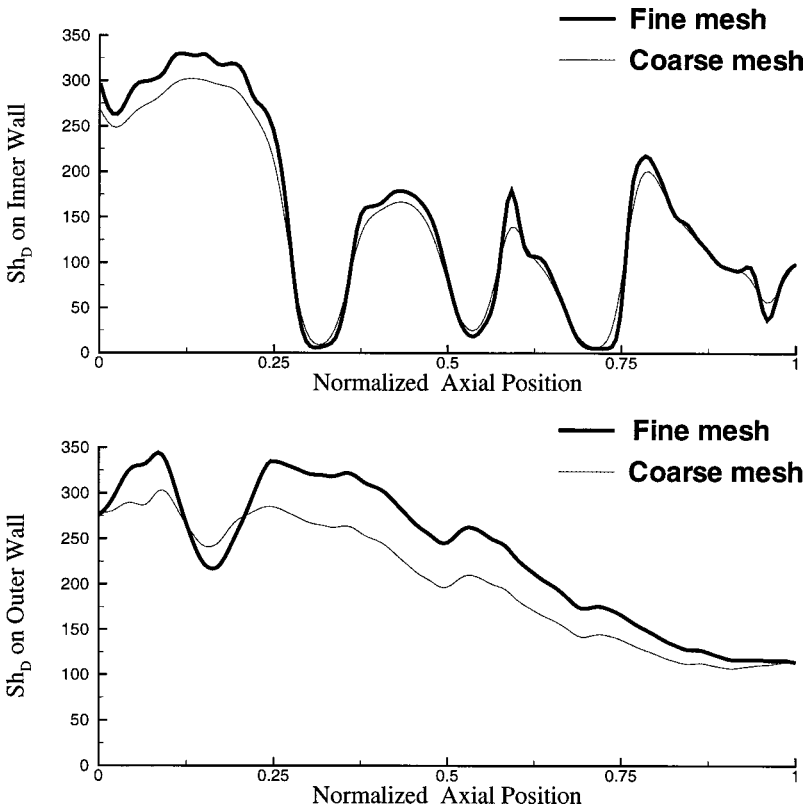

FIGURE 4. Grid sensitivity study in mass transfer calculations: Sh_D distributions on the inner wall (top panel) and outer wall (bottom panel) for two different meshes.

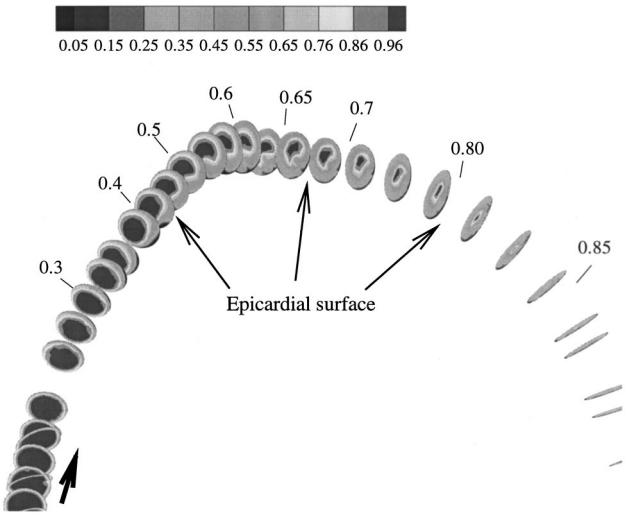

FIGURE 5. Isoconcentration contours along the arterial length. The numbers are the distances along the artery as normalized by the total artery length. Re_D=500 and Sc=3000.

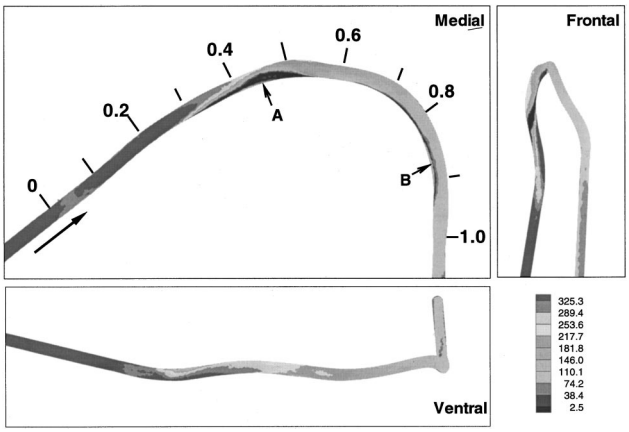

FIGURE 7. Sherwood number distribution on the RCA walls. The numbers are the distances along the artery as normalized by the total artery length. Labels A and B point to areas of low Sherwood number. Re_D=500 and Sc=3000.

that mass transfer was being strongly influenced by secondary flow effects. In order to better understand such effects, the hemodynamics at two locations within the proximal region, namely 31% and 42% of the distance along the artery (see Fig. 6), were examined in detail. At the 31% station, the cross-sectional area is increasing [see Fig. 2(c)] and as a result the flow is decelerating and

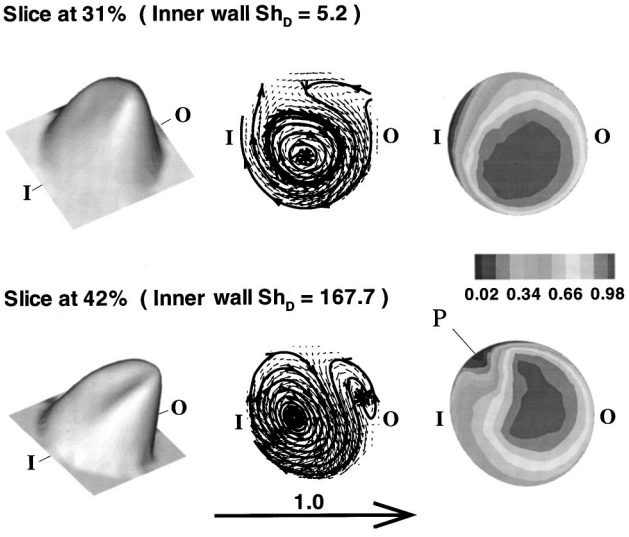

FIGURE 6. Velocity profile (left panels), secondary flow features (center panels), and concentration profile (right panels) at two different locations, namely 31% and 42% along the RCA model length. These two locations experience low and high Sh_D, respectively. Labels I and O refer to inner and outer walls, respectively. Label P in the bottom right panel refers to a low concentration fluid that accumulates as a result of the interaction between two counter-rotating Dean cells. Heavy lines in middle panel are ''sectional streamlines'' (constrained to lie in the plane of the figure).

the relative effect of secondary flows is more significant. A fairly large deviation from the medial plane is exhibited by the geometry at this station [see Fig. 2(b)]. The unmatched Dean vortex structure due to primary curvature of the artery is pulled away from the inner wall (see the top middle panel in Fig. 6). At this station, the second Dean cell (not shown in the figure) is very weak. The concentration field is thus pulled away from the inner wall, leaving a low concentration region near the inner wall.

As we move from station 31% to station 42%, the secondary curvature of the artery changes direction [see Fig. 2(b)] and the local Dean number increases (see Fig. 3). At the same time, the matching second Dean cell grows and pushes the dominant Dean cell towards the inner wall. As a result, low concentration fluid is pushed away from the inner wall, and high concentration fluid redistributes itself near the inner wall. The smaller counter-rotating Dean cell near the outer wall distributes the high concentration fluid near the outer wall as well. As a result of the interaction of these two vortices, a secondary flow separation region occurs on the upper (side) wall, and low concentration fluid accumulates in this region (see Fig. 6, label P in the bottom right panel).

Sherwood Number Distribution. The dimensionless concentration gradient (Sherwood number) on the artery wall is shown in Fig. 7. As the blood enters the primary curvature (i.e., in the medial plane) of the RCA, the Sherwood number on the outer wall is increased, with a decreased Sherwood number on the inner wall. This general trend persists throughout the artery, consistent with the wall shear stress patterns in this geometry. However, as shown in Fig. 7, the high and low Sherwood regions ''twist'' circumferentially in response to changes in the secondary flow patterns induced by the secondary curva-

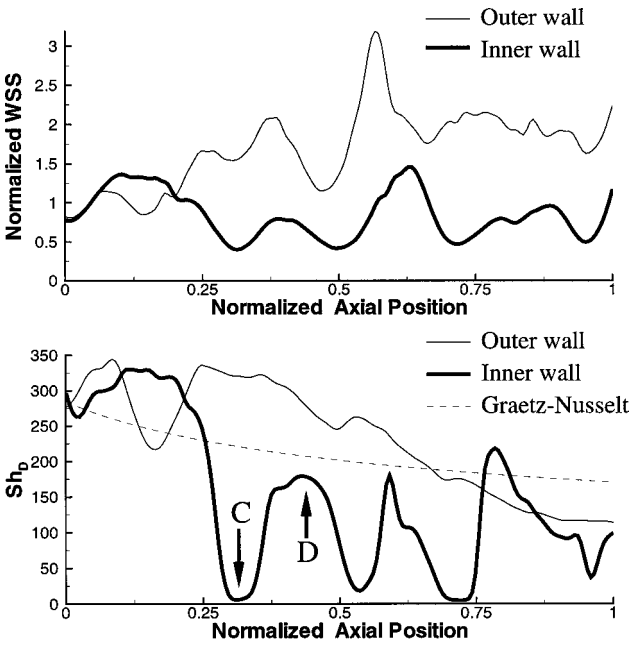

FIGURE 8. Distribution of normalized WSS and Sh_D along the RCA. The WSS values are normalized by the WSS in fully developed flow in a pipe with similar inlet diameter. The arrows in the Sh_D plot refer to stations at 31% and 42% distance along the artery. The inner and outer walls refer to the surfaces closest to and farthest from the heart. The dashed line is the Sh_D distribution expected for a developing mass transfer boundary layer in a straight tube with inlet radius a (Graetz–Nusselt solution).

ture of the artery. This ''twisting'' of the mass flux patterns is superimposed on the dominant flux patterns determined by the primary curvature of the RCA. The result is that local Sh_D varies substantially, particularly on the inner wall (see Fig. 8). Such Sh_D variations on the inner wall occur sporadically in localized areas along the arterial length, as secondary curvature effects push the high concentration fluid towards and away from this wall. This also creates significant side wall variations in mass flux.

Further insight into local Sh_D variations can be obtained from Fig. 8. The arrows labeled C and D in this plot refer to stations 31% and 42% that were examined in the Isoconcentration Contours section. As discussed earlier, at station 31% the high concentration fluid is shifted away from the inner wall. As a result, low concentration fluid accumulates near the inner wall, hence, a low Sherwood number is experienced on the inner wall. At station 42%, the secondary flow causes the high concentration fluid to distribute itself near the inner and outer walls. Hence, both inner and outer wall locations experience high Sh_D at this location (arrow D in Fig. 8).

As evident in Fig. 8, the Sh_D on the inner wall has a pattern of peaks and valleys similar to that seen for the wall shear stress (WSS), but of much higher relative magnitude. Considering only the data on the inner and outer walls, the maximum/minimum ratio for normalized WSS was approximately 8, while this ratio for Sh_D was about 54. This observation can be explained as follows. The momentum transfer sees a diffusivity (kinematic viscosity) that is three orders of magnitude greater than the mass transfer diffusivity. Thus, variations are more effectively ''diffused away'' in momentum transport, leading to lower WSS variations. Over the entire model (i.e., not restricting comparison to only the inner and outer walls), the maximum/minimum ratio for Sh_D was about 112.

The variation in Sh_D along the outer wall is small and relatively smooth. The peaks and valleys in the outer wall Sh_D plot do not follow the trend seen in the outer wall WSS plot. This may in part be due to mesh resolution issues near the outer wall.

SUMMARY AND CONCLUSIONS

Fluid flow and mass transfer patterns were calculated in a human right coronary artery model with a realistic geometry. The concentration field within RCA was seen to closely follow primary and secondary flow features. The variations in fluid flow and mass transfer patterns due to the variations in the arterial geometry appeared significant. The secondary curvatures drive circumferential shifts in the location of the Dean cells created as a result of primary curvatures of the arterial geometry. As a result of this, regions of high and low Sherwood numbers were superimposed on the dominant flux patterns determined by the primary curvature of the RCA. These low and high Sherwood number regions twist around the artery in response to the secondary curvature. Consequently, the local Sherwood number varies by nearly two orders of magnitude from inner to outer wall.

These results are in general agreement with data presented by Qiu and Tarbell,[18] who showed large local variations in Sherwood number in a planar curved tube model with constant curvature and constant circular cross section. They reported a maximum value of steady-flow Sherwood number on the outer wall of approximately 80, and a minimum value on the inner wall of approximately 0.1. This 800-fold variation in Sh_D was reduced to approximately 23 fold by the addition of flow pulsatility and diameter variation. It is possible that flow pulsatility and elastic wall deformation would also reduce the maximum range of Sherwood numbers seen in our realistic model. Further work is required to investigate this issue.

For steady flow conditions, we saw a range of Sh_D values of about 110 (maximum value divided by minimum value) in our model. This is about a seven-fold smaller range than reported by Qiu and Tarbell's for steady flow in their ideal geometry. We believe that this difference is largely due to enhanced mixing resulting from the more complex secondary flows that are present

in the realistic model. In other words, complex geometric features may act to reduce the local variations in Sh_D, as compared to the situation in an ideal geometry. However, the local geometric features also create a complex pattern of local maxima and minima in Sh_D. Such local mass transport features are:

(1) not easily predicted *a priori*;
(2) much larger than the corresponding local variations in wall shear stress; and
(3) potentially important for understanding the pathogenesis of atherosclerotic lesions.

We conclude that anatomically realistic, patient-specific arterial models are needed before any conclusion is drawn about possible links between local mass transport variations and atherosclerosis. Further experimental studies of mass transfer effects on arterial wall biology are also required.

ACKNOWLEDGMENTS

This work was supported by NSERC E. W. R. Steacie Fellowship (CRE). The authors thank Dr. M. Ojha for making the RCA model available to them and Dr. J. Moore for constructing the CAD model. M. Kaazempur-Mofrad acknowledges fruitful discussions with Dr. J. Myers.

REFERENCES

[1] Ballyk, P. D., D. A. Steinman, and C. R. Ethier. Simulation of non-Newtonian blood flow in an end-to-side anastomosis. *Biorheology* 31:565–586, 1994.
[2] Caro, C. G., J. M. Fitz-Gerald, and R. C. Schroter. Observation, correlation and proposal of a shear dependent mass transfer mechanism for atherogenesis. *Proc. R. Soc. London, Ser. B* 177:109–159, 1971.
[3] Crawford, D. W., and D. H. Blankenhorn. Arterial wall oxygenation, oxyradicals and atherosclerosis. *Atherosclerosis* 39:97–108, 1991.
[4] Dull, R. O., J. M. Tarbell, and P. F. Davies. Mechanism of flow-mediated signal transduction in endothelial cells: Kinetics of ATP surface concentrations. *J. Vasc. Res.* 29:410–419, 1992.
[5] Frangos, S. G., V. Gahton, and B. Sumpio. Localization of atherosclerosis: Role of hemodynamics. *Arch. Surg.* 134:1142–1149, 1999.
[6] Friedman, M. H., P. B. Baker, Z. Ding, and B. D. Kuban. Relationship between the geometry and qualitative morphology of the left anterior descending coronary artery. *Atherosclerosis* 125:183–192, 1996.
[7] Friedman, M. H., G. M. Hutchins, C. B. Bargeron, O. J. Deters, and F. F. Mark. Correlation between intimal thickness and fluid shear in human arteries. *Atherosclerosis* 39:425–436, 1981.
[8] He, X., and D. N. Ku. Pulsatile flow in the human left coronary artery bifurcation: Average conditions. *ASME J. Biomech. Eng.* 118:74–82, 1996.
[9] Kaazempur-Mofrad, M. R. A characteristic/finite element algorithm for 3D unsteady advection-dominated transport phenomena using unstructured grids. PhD thesis, Department of Mechanical and Industrial Engineering, University of Toronto, 1999.
[10] Kaazempur-Mofrad, M. R., and C. R. Ethier. An efficient characteristic Galerkin scheme for the advection equation in 3D. *Comp. Meth. Appl. Mech. Eng.* (submitted).
[11] Kaazempur-Mofrad, M. R., P. D. Minev, and C. R. Ethier. A characteristic/finite element algorithm for 3D unsteady advection-dominated transport phenomena using unstructured grids. *Comp. Meth. Appl. Mech. Eng.* (submitted).
[12] Ku, D. N., D. P. Giddens, K. Z. Christopher, and S. Glagov. Pulsatile flow and atherosclerosis in human carotid bifurcation. *Atherosclerosis* 5:293–302, 1985.
[13] Myers, J. G., J. A. Moore, M. Ojha, K. W. Johnston, and C. R. Ethier. Factors influencing blood flow patterns in the human right coronary artery. *Ann. Biomed. Eng.* 29:109–120, 2001.
[14] Nollert, M. U., and L. V. McIntire. Convective mass transfer effects on the intracellular calcium response of endothelial cells. *ASME J. Biomech. Eng.* 114:321–326, 1992.
[15] Ojha, M., R. L. Leask, J. Butany, and K. W. Johnston. Distribution of intimal and medial thickening in the human right coronary artery: A study of 17 RCAs. *Atherosclerosis* (in press).
[16] Patel, B. R. Internal flows. In Handbook of Fluid Dynamics and Fluid Machinery, edited by J. A. Schetz and A. E. Fuhs, Southampton, UK: Wiley, 1996, Chap. 5.
[17] Pedley, T. J. The Fluid Mechanics of Large Blood Vessels. Cambridge: Cambridge University Press, 1980.
[18] Qiu, Y., and J. M. Tarbell. Numerical simulation of oxygen mass transport in a compliant curved tube model of a coronary artery. *Ann. Biomed. Eng.* 28:26–38, 2000.